Study charge carriers diffusion in field free silicon

Mikhail Smirnov, Department of Electrical and Computer Engineering,

New York Institute of Technology, New York, NY 10023

Ivan Kotov, Instrumentation Division, Brookhaven National Laboratory, Upton, NY, 11973

Abstract

The National Synchrotron Light Source II (NSLS-II) Soft Inelastic x-ray Scattering (SIX beamline) at Brookhaven National Laboratory (BNL) includes two Electron-Multiplying Charge-Coupled Devices (EMCCDs) for x-ray detection. These devices work by converting beams of photons into electrons captured by pixel gates that are then converted into a voltage to create images of the incident x-rays. On the way to the pixel gates, the electrons drift in the depletion zone and diffuse in the field-free region. The diffusion of charges in the field-free region is important to model as it affects the readout. This work examines the diffusion of charges in EMCCDs using mathematical modeling and computational simulation in the C++ ROOT framework. Being able to theoretically predict charge diffusion will allow us to develop EMCCDs with better accuracy in coordinate measurements for x-rays. One way we can better describe the charge distribution shape is by modeling the electron cloud with a Gaussian shape instead of a simple point charge with the Dirac delta function. From gaining a better understanding of EMCCD charge diffusion, x-ray measurement at BNL's NSLS-II can be done more accurately, in addition to improving upon other EMCCD applications, such as in astronomy, medical imaging, and optical microscopy.

I. Introduction

A CCD (Charge-Coupled Device) is an integrated circuit containing metal-oxide-silicon (MOS) structures divided up into pixels. Each pixel allows for conversion from photons into electron-hole pairs. CCDs are commonly used as sensors for digital imaging by transferring charge between their pixels. Each pixel contains gates (electrodes) in which voltages can be applied to in order to create potential wells under each electrode. The gates are used to shift the charges along columns of pixels and and then get collected into a serial register. Each pixel in each line of the image shifts its charge to the sense node and the energy of the photons hitting the pixels dictates how many electron-hole pairs are generated. Since the intensity of the incident rays is proportional to

the amount of electron-hole pairs, the resulting amount of collected electrons allows for measurement of the incident rays. In this case, CCDs are used for x-ray detection at BNL's NSLS II's SIX beamline[1] with pixel size being 16 μm and the total device thickness being approximately $14\mu m$. The first $8\mu m$ of width in the back side of the EMCCD is the field-free region, while the depletion layer is $6 - 8\mu m$ thick. The total imaging area spans 1632 columns and 1608 rows of pixels. The electrons are collected under electrode gates where a potential well is formed. In addition, a specific type of CCD known as, Electron-Multiplying Charge-Coupled Devices (EMCCDs), multiply electrons by impact ionization. This added stage allows for CCDs with greater sensitivity and lower readout noise.

A typical CCD model consists of multiple layers: the depletion layer, the field-free region and the reflective boundary at the entrance window. An x-ray beam is incident on the depletion region and the created electron hole pairs diffuse in the field-free region until they get reflected at either the entrance window or until they reach the interface between the field-free and depletion regions. The depletion region is described as the area where charges from x-rays are absorbed and travel towards the nearest potential well. The area underneath, the field-free region, does not experience an electric field but instead the charges migrate by diffusion[2]. Understanding the diffusion of charges in the field-free region allows for a more accurate prediction of x-rays, resulting in better coordinate accuracy when measuring x-rays with CCDs.

II. Scope and Objectives

This work models the diffusion of charges in the field-free region of an EMCCD by first incorporating the diffusion equation with a boundary value problem at the boundaries between the top of the EMCCD (the interface between the depletion zone and the field free region) and the bottom of the EMCCD (the reflective entrance window boundary). In previous works[1,3], typically the initial charge cloud distribution was modeled by the Dirac delta function, which represented a single point of charge at the very center of the pixels. However, a more practical and realistic example is to use the Gaussian function to model the initial spread of charges. For this reason,

this work compares the equations for charge density when incorporating these two different initial conditions. Afterwards, this work aims to calculate and plot the charge distribution on the EMCCD pixels in the field-free region accurately. This is done by computing the charge distribution function, calculated with the Gaussian function initial condition, by numerically solving the equation using C++ and plotting the resulting histograms in ROOT.

III. Methods

A. Diffusion Equation

In order to model the diffusion in the field-free region of CCD's, we follow the process in [4] and introduce the three-dimensional diffusion equation in cylindrical coordinates and assume axisymmetric symmetry,

$$D\nabla^2\rho(\mathbf{r},z,t) = \frac{\partial\rho(\mathbf{r},z,t)}{\partial t}, \tag{1}$$

where ρ is the charge density and D is the diffusivity, with the radial and axial directions, $(\mathbf{r},z)$. The radial direction, $\mathbf{r}$, is defined as, $\mathbf{r} = (x,y)$ from the origin (x_0,y_0), while the axial direction, z, describes the depth of the CCD.

We set $z = 0$ to be the top of the sensor (the depletion zone interface) and $z = h$ to be the reflective entrance window boundary. We assume no accumulation of charges at the depletion zone interface and assume no flux of charges through the reflective entrance window. In total the two boundary conditions are,

$$\rho(\mathbf{r},z,t)\Big|_{z=0} = 0, \quad \frac{\partial\rho(\mathbf{r},z,t)}{\partial z}\Big|_{z=h} = 0. \tag{2}$$

i. Dirac Delta Function as an Initial Condition

To solve this boundary value problem we take the solution[4] which considered the Dirac delta initial condition, $\rho(\mathbf{x},0) = \delta(\mathbf{x}-\mathbf{x_0})$. Considering the vectors are n-dimensional, the solution for

the charge density is found to be the following for each vector component,

$$\boxed{\rho(\mathbf{x},t) = \frac{1}{(2\pi)^n}\int_{-\infty}^{\infty} e^{-Dt\sum k_j^2} e^{-i\sum k_j(x_j - x_j^0)} \prod dk_j} \\ \boxed{= \frac{1}{(4\pi Dt)^{n/2}} \exp\Big[-\frac{(\mathbf{x}-\mathbf{x}_0)^2}{4Dt}\Big]}, \tag{3}$$

where $k = \frac{u}{\sqrt{Dt}}$.

The boundary conditions (2) are then applied to the general solution, which results in the following equation for the solution with the Dirac delta function initial condition,

$$\boxed{Z(z')T(t) = 2\sum_{n=0}^{\infty} \sin(\alpha_n \cdot z_0') \sin(\alpha_n \cdot z') \exp\Big(-\frac{\alpha_n^2 Dt}{h^2}\Big)}, \tag{4}$$

where $\alpha_n = (n+\frac{1}{2})\pi$ and z' is the coordinate normalized by the height of the EMCCD, $z' = \frac{z}{h}$.

ii. Gaussian Function as an Initial Condition

If we instead assume the Gaussian function as the initial condition, $\rho(\mathbf{x},t)\Big|_{t=0} = Ae^{-\frac{(\mathbf{x}-x_0)^2}{2\sigma^2}}$,

$$\rho(\mathbf{k},0) = \frac{1}{2\pi}\int_{-\infty}^{\infty} Ae^{-\frac{(\mathbf{x}-x_0)^2}{2\sigma^2}} e^{i\mathbf{k}\mathbf{x}} d\mathbf{x}, \tag{5}$$

where $\rho(\mathbf{k},0)$ is the Fourier transform of the initial condition of the charge density, we can plug the above equation into the following differential equation solution,

$$\rho(\mathbf{k},t) = \rho(\mathbf{k},0)e^{-Dk^2t}. \tag{6}$$

This results in

$$\rho(\mathbf{k},t) = \frac{1}{2\pi} e^{-Dk^2t} A\int_{-\infty}^{\infty} e^{-\frac{(\mathbf{x}-x_0)^2}{2\sigma^2} + i\mathbf{k}\cdot\mathbf{x}} d\mathbf{x}, \tag{7}$$

and if $A = \frac{1}{\sqrt{2\pi}\sigma_0}$ for the normalized Gaussian function, along with σ being notated as σ_0, the

equation simplifies to

$$\rho(\mathbf{k},t) = \frac{1}{2\pi} e^{-Dk^2t + ix_0\mathbf{k} - \frac{k^2\sigma_0^2}{2}}. \tag{8}$$

Taking the inverse Fourier transform,

$$\rho(\mathbf{x},t) = \frac{1}{2\pi}\int_{-\infty}^{\infty} e^{-[(Dt+\frac{\sigma_0^2}{2})k^2 + (-ix_0 + i\mathbf{x})\mathbf{k}]} d\mathbf{k}, \tag{9}$$

$\sigma(t) = \sigma = \sqrt{2Dt + \sigma_0^2}$ is defined for simplicity. Normalized variables are also used which were scaled by the height of the EMCCD, $D' = \frac{D}{h^2}$ and $\sigma_0' = \frac{\sigma_0}{h}$.

We perform the integration and using the definition of the error function, $(\mathrm{erf}(z) = \int_0^z \frac{2e^{-u^2}}{\sqrt{\pi}} du)$, we finally arrive at the solution for n-dimensions for the charge density using the Gaussian function initial condition,

$$\boxed{\rho(\mathbf{x},t) = \left(\frac{e^{-\frac{(\mathbf{x}-x_0)^2}{2\sigma^2}}}{\sqrt{2\pi}\sigma}\right)^n}, \tag{10}$$

along with the normalized solution,

$$\boxed{\rho(\mathbf{x},t) = \left(\frac{e^{-\frac{(\mathbf{x}'-x_0')^2}{2\sigma'^2}}}{\sqrt{2\pi}\sigma'}\right)^n}. \tag{11}$$

Similar to the Dirac delta function initial condition, we apply the boundary conditions (2) to the general solution, this time with the Gaussian function. The Gaussian function initial condition solution is obtained as the following,

$$\boxed{Z(z')T(t) = \mathrm{erf}(1)\sum_{n=0}^{\infty} e^{-\frac{\alpha_n^2}{2}({\sigma_0'}^2 + 2D't)} \sin(\alpha_n z_0') \sin(\alpha_n z').} \tag{12}$$

iii. Charge Distribution

By investigating the charge flux at the boundary between the field-free region and depletion region (at $z = 0$) integrated over time, we are able to obtain the distribution of charges,

$$q(\mathbf{r}) = D \int_0^\infty \frac{\partial \rho}{\partial z}\Big|_{z=0} dt. \tag{13}$$

We take the solution from [3],

$$\rho(\mathbf{r}, z, t) = \frac{Q_0}{4\pi Dth} \cdot 2 \sum_{n=1}^{\infty} \sin(\alpha_n z_0') \sin(\alpha_n z') \exp\Big(- \frac{\alpha_n^2 Dt}{h^2} - \frac{r^2}{4Dt}\Big), \tag{14}$$

and take the derivative with respect to z,

$$\frac{\partial \rho(\mathbf{r}, z, t)}{\partial z}\Big|_{z=0} = \frac{Q_0}{4\pi Dth^2} \cdot 2 \sum_{n=1}^{\infty} \alpha_n \sin(\alpha_n z_0') \exp\Big(- \frac{\alpha_n^2 Dt}{h^2} - \frac{r^2}{4Dt}\Big) \tag{15}$$

The charge, q_j, in each pixel, j, can be obtained by integrating the flux at the depletion zone boundary over both the pixel area and over time. This is done by integrating (15) in Cartesian coordinates, (x, y) and by integrating over time, t, such as in (13). Following this process in normalized coordinates, we arrive at

$$\begin{aligned} q_j &= D \int_0^\infty \int_A^B \int_C^E \frac{Q_0}{4\pi Dth^2} 2 \sum_{n=0}^{\infty} \alpha_n \sin(\alpha_n z_0') \exp(-\frac{\alpha_n^2 Dt}{h^2} - \frac{r^2}{4Dt}) dx dy dt, \\ q_j &= \frac{Q_0}{2} \int_0^\infty \int_A^B \int_C^E \frac{1}{\pi} \sum_{n=0}^{\infty} \alpha_n \sin(\alpha_n z_0') \exp(-\frac{\alpha_n^2}{4}\sigma^2 - \frac{r'^2}{\sigma^2}) d(\frac{x'}{\sigma}) d(\frac{y'}{\sigma}) d\sigma^2, \end{aligned} \tag{16}$$

where $\sigma^2 = \frac{4Dt}{h^2}$. Note that A and B are the x-coordinates representing the start and end of each pixel while C and E are the y-coordinates representing the start and end of each pixel. The center of the grid is represented by (x_0, y_0) which is considered to be $(0, 0)$. In addition, the coordinates are all normalized by the height, ($x' = \frac{x}{h}$, $y' = \frac{y}{h}$, $z' = \frac{z}{h}$, $\mathbf{r}' = \frac{r}{h}$).

Looking at only the spatial integral over area, we have

$$\boxed{p_j = \frac{1}{4}\left(\operatorname{erf}(\frac{b}{\sigma}) - \operatorname{erf}(\frac{a}{\sigma})\right)\left(\operatorname{erf}(\frac{e}{\sigma}) - \operatorname{erf}(\frac{c}{\sigma})\right)}, \tag{17}$$

which results in the entire integral including integration over time,

$$\boxed{q_j = \frac{Q_0}{2}\sum_{n=0}^{N}\alpha_n \sin(\alpha_n z_0')\int_0^{\infty}\exp\left(-\frac{\alpha_n^2}{4}\sigma^2\right)\cdot p_j\Big(\frac{1}{\sigma}\Big)d\sigma^2}, \tag{18}$$

as $N \to \infty$, $\alpha_n = (n + \frac{1}{2})\pi$, and the rectangular pixel borders are at $x = [a, b]$ and $y = [c, e]$.

This charge distribution function is evaluated along a 5 x 5 grid of square pixels, with the x and y coordinates being scaled to from -5 to 5 and a pixel size of 2 x 2 dimensionless units. Equations (17) and (18) will together demonstrate the charge distribution in the field free region (at $z_0' = 1$) with the initial cloud charge, $Q_0 = 1$, along the EMCCD grid.

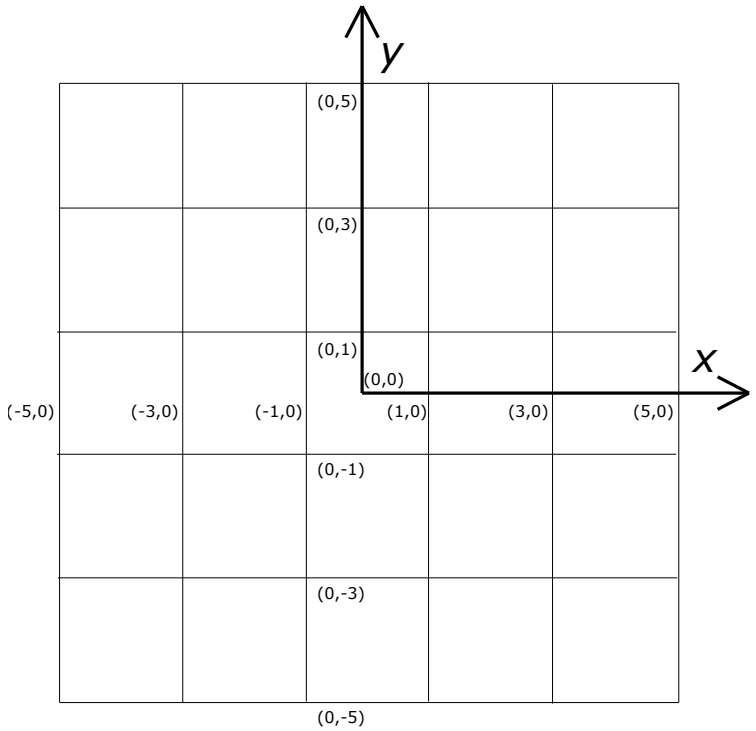

Figure 1: A 5x5 grid used to represent the pixels and their respective coordinates of the EMCCD.

B. Numerical Integration

In order to evaluate and plot (18), we perform three different integration methods: Midpoint Rule, Trapezoidal Rule, and Simpson's Rule. In general, the Midpoint Rule approximates curves using straight horizontal lines from rectangles, the Trapezoidal Rule approximates curves using ramped straight lines from each trapezoid's leg, and the Simpson's Rule approximates curves using quadratic curves. Therefore, especially when it comes to more complicated functions, the Midpoint Rule provides the least accurate approximation while Simpson's Rule provides the most accurate approximation for an integral.

i. Midpoint Rule

The midpoint between any two points, $f(a)$ and $f(b)$, of a function, $f(x)$, is calculated by

$$\frac{f(a)+f(b)}{2},$$

which allows for numerical integration using the midpoints of the subintervals of a function.

The Midpoint Rule states that a definite integral over an interval, $[a,b]$, can be approximated by dividing the area under a function, $f(x)$, into n subintervals of equal width, Δx, and summing up the midpoints between each subinterval. The area between each subinterval is approximated by a rectangle. The Midpoint Rule is defined by

$$\int_a^b f(x)dx \approx \Delta x[f(x_1^*)+f(x_2^*)+...+f(x_n^*)], \tag{19}$$

where $\Delta x = \frac{b-a}{n}$ is the width of n subintervals, and x_i^* is the midpoint of each subinterval, x_i.

ii. Trapezoidal Rule

Similar to the Midpoint Rule, the area under a function, $f(x)$, is split up into n subintervals over the interval $[a,b]$. However, instead of rectangles, the subintervals are composed of trapezoids

whose legs try to approximate the curve with straight slanted lines. The area of a trapezoid is given by,

$$\left(\frac{A+B}{2}\right)H,$$

where A and B are the bases of the trapezoid and H is the height of the trapezoid. This concept can therefore be used to obtain the formula for the Trapezoidal Rule,

$$\int_a^b f(x)dx \approx \frac{\Delta x}{2}[f(x_0) + 2f(x_1) + 2f(x_2) + ... + 2f(x_{n-1}) + f(x_n)], \tag{20}$$

where $\Delta x = \frac{b-a}{n}$ is the width of n subintervals, and x_i is the point of each subinterval, x_i.

iii. Simpson's Rule

Instead of approximating the curve with straight lines as with the Trapezoidal Rule, the function can be approximated with a quadratic function that has to agree with three points from the subintervals using Simpson's Rule.

For example, the area under the approximation on the intervals, $[x_{i-1}, x_i]$ and $[x_i, x_{i+1}]$, would be given by

$$\frac{\Delta x}{3}[f(x_{i-1}) + 4f(x_i) + f(x_{i+1})].$$

By incorporating n subintervals, the general equation for Simpson's Rule is defined by,

$$\int_a^b f(x)dx \approx \frac{\Delta x}{3}[f(x_0) + 4f(x_1) + 2f(x_2) + ... + 2f(x_{n-2}) + 4f(x_{n-1}) + f(x_n)], \tag{21}$$

where $\Delta x = \frac{b-a}{n}$ is the width of n subintervals, and x_i is the point of each subinterval, x_i.

IV. Results

A 2D plot (Figure 2) of the charge distribution time integral at the center pixel is shown in order to demonstrate the overall behavior of the integral. The function is continuous along the entire domain and converges quickly past approximately $\sigma = 4$. The plot overall resembles a function similar to a Gaussian curve, due to the close relationship between the error function and the Gaussian function. Since the time integral is bounded from 0 to ∞ and rapidly converges, the bounds from the integral are approximated to be from 0 to 10 in order to be numerically solved.

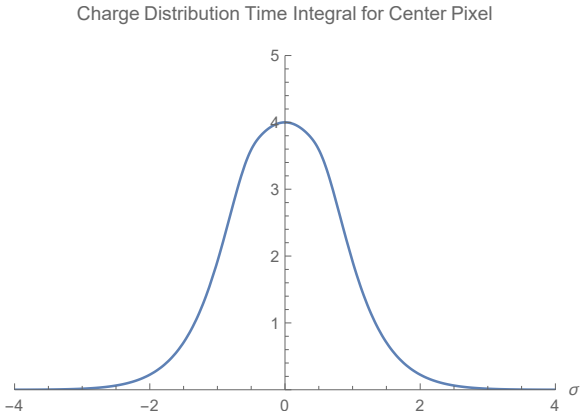

Figure 2: Plot of charge distribution time integral term for center pixel.

To compare the accuracy of the various numerical integration methods of the time integral, the charge distribution is plotted for $n = 0$ in the summation (Figure 3). The integral is evaluated three different times from 0 to 10 with 10 subintervals using the Midpoint Rule, the Trapezoidal Rule, and Simpson's Rule. Due to the values around the center pixels rapidly decreasing, the functions were plotted on a logarithmic scale. The shapes of the plots are very similar, meaning that the different integration methods do not have a significant impact on the plot. However, based on the central pixel values, as well as some of the surrounding pixel values, Simpson's Rule produced slightly more accurate values. The Midpoint Rule and Trapezoidal Rule plots are identical in values, meaning that the quadratic approximation from the Simpson's Rule plot matches the curve more accurately. As the function shown in Figure 2 has a steep curvy shape, a quadratic approximation instead of a linear approximation for its integral would be more accurate. For the sake of

simplicity and accuracy, the rest of the results for the charge distribution will be shown using only Simpson's Rule.

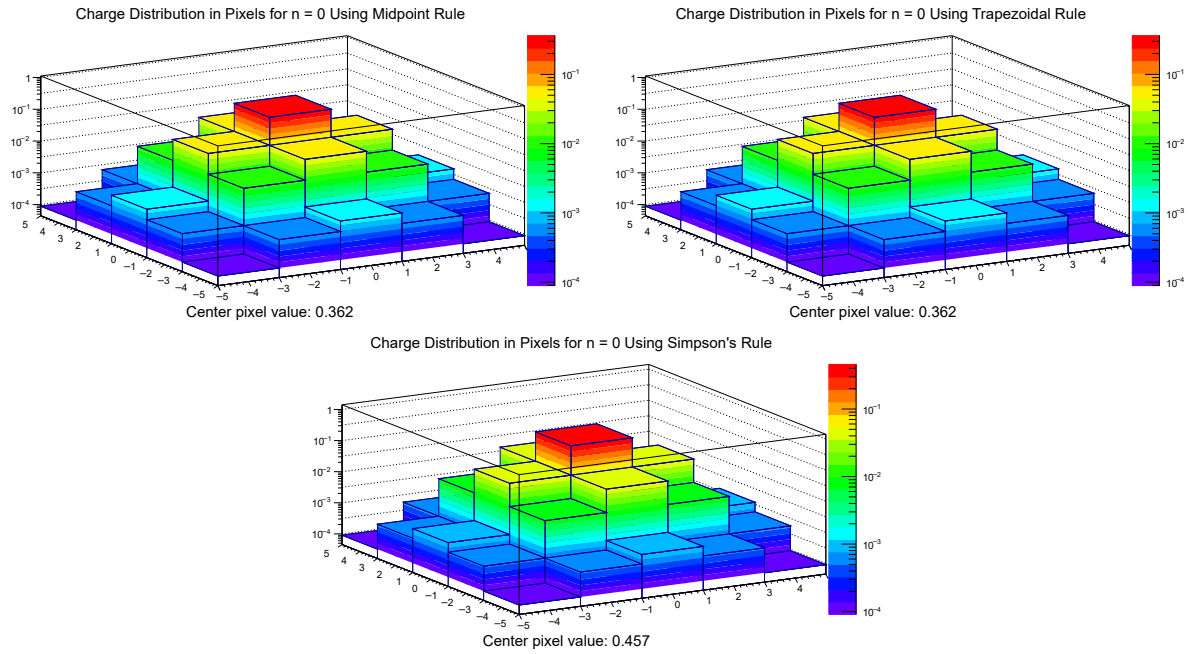

Figure 3: Comparison of evaluating the charge distribution integral with the Midpoint Rule, Trapezoidal Rule, and Simpson's Rule.

The full charge distribution function is plotted for different summation limits, N, using a logarithmic scale in Figure 4. For the purpose of demonstration, each of the values are also scaled by the center pixel value, meaning that the center pixel value is normalized to 1. For most accuracy, the number of subintervals in the numerical integration is 1000. Each summation for each value of n in the charge distribution function decreases, meaning that the summation converges very quickly. As large values of n would produce infinitesimal values, the shape and values of the plots change by only a very small factor. Due to this, the plots are not graphed past the summation limit of $N = 100$, as the values converge and do not produce any significant differences at higher limits. Each of the plots show an expected 3D Gaussian curve shape along the center pixel with symmetry along $x = 0$ and $y = 0$. The values quickly decrease logarithmically around the center pixel, while the center pixel maintains its maximum value. The charge distribution is therefore centered along the center pixel and spreads radially with gradual values.

The full charge distribution is also plotted on a linear scale in Figure 5 to demonstrate the

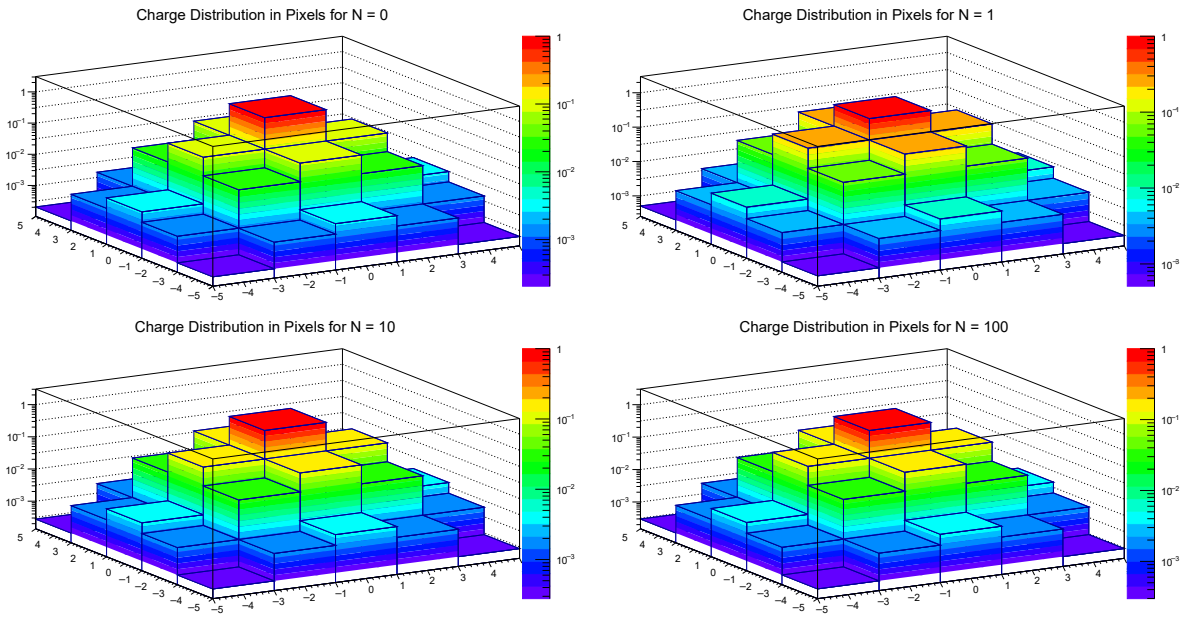

Figure 4: Charge distribution plots for different summation limits.

large concentration of charges in the center pixel. The summation limit is $N = 100$ with 1000 subintervals used in the numerical integration and the values are scaled by the center pixel value similar to Figure 4. This plot provides a practical view of the charge distribution and shows the rapid drop in values at the pixels neighboring the center pixel. With the z-axis not being on a logarithmic scale, the 3D Gaussian shape becomes much thinner but still keeps its symmetry and behavior on a linear scale.

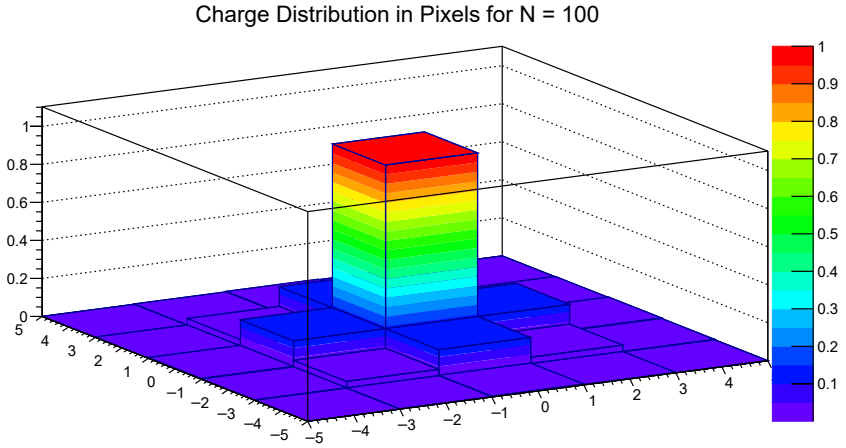

Figure 5: Charge distribution for $N = 100$ on a non-logarithmic scale.

V. Conclusion

After evaluating the charge distribution function, (18), the distribution of charges on the surface of the EMCCD sensor was able to be demonstrated. Since the initial condition for the initial electron cloud shape was modeled by a Gaussian function, the plots having a similar Gaussian shape match with the initial predictions. In addition, the charge density functions for both the Dirac delta function initial condition and the Gaussian function initial condition were solved for, which showed that a Gaussian function is a more natural and realistic approximation for the initial charge distribution instead of having the Dirac delta function at the center of the pixels model a single point charge. The time integral and summation of the charge distribution function both converge rapidly at low values, meaning that evaluating the charge distribution function does not require a lot of computation and that the function is well-behaved. Also, despite the various integration methods, all three of them produced very similar results, however Simpson's Rule was still the most accurate as it approximated the curve quadratically. Each of the histograms show that the charges are most focused in the center pixel as the x-ray beam is incident on the center of the 5x5 grid of pixels, and the charges spread out symmetrically at small values. These results provide a more accurate function to predict charge distribution and measure x-ray coordinates that can be used in applications of the NSLS-II SIX beamline, as well for other various EMCCD uses.

VI. Acknowledgements

First, I would like to acknowledge my mentor, Ivan Kotov, for providing invaluable guidance throughout this project and granting me the opportunity to work on this project that allowed me to further improve my research skills. Secondly, I want to thank my intern collaborator, Andrea Houck, who provided great assistance to parts of this research, such as the mathematical modeling, as we both worked together on similar parts of the project. Lastly I would like to acknowledge the U.S. Department of Energy Office of Science and BNL's Office of Educational Programs, as this project was supported in part by the U.S. Department of Energy, Office of Science, Office of

Workforce Development for Teachers and Scientists (WDTS) under the Science Undergraduate Laboratory Internships Program (SULI).

VII. References

[1]I. Kotov, S. Hall, D. Gopinath, A. Barbour, J. Li, Y. Gu, K. Holland, A. Holland, I. Jarriage, J. Pelliciari, M. Soman, S. Wilkins, and V. Bisogni, "Analysis of the EMCCD point-source response using x-rays", Nuclear Inst. and Methods in Physics Research, A: Accelerators, Spectrometers, Detectors and Associated Equipment, **985**, 164706 (2021).

[2]G. R. Hopkinson, "Charge diffusion effects in CCD x-ray detectors", Nuclear Instruments and Methods **216**, 423-429 (1983).

[3]George G. Pavlov, "Charge diffusion in CCD X-ray detectors." Nuclear Instruments and Methods in Physics Research Section A: Accelerators, Spectrometers, Detectors and Associated Equipment, **428**(2-3), 348-366 (1999).

[4]I. Kotov, "Diffusion in the field-free zone", (private communication) (2021).